ON THE EFFECT OF QUORUM SENSING AND DELAY IN COUPLED NONLINEAR DEGENERATE OPTICAL PARAMETRIC OSCILLATORS

Papri Saha

Department of Physics, B.P. Poddar Institute of Management and Technology
137 VIP Road, Kolkata 700052, India
papri.saha@gmail.com

Anirban Ray

Department of Physics, Gour Mahavidyalaya
Mangalbari, Malda 732142, West Bengal, India
anirban.chaos@gmail.com

A. Roy Chowdhury

High Energy Physics Division, Department of Physics, Jadavpur University
188, Raja Subodh Chandra Mallick Road, Kolkata 700032, West Bengal, India
asesh_r@yahoo.com

(Received July 24, 2017; accepted September 26, 2017)

Complex dynamical structures inherent in degenerate optical parametric oscillator (DOPO) system are studied in detail. The system under consideration is actually the temporal part of the original DOPO system. A host of fixed points and the corresponding route to chaos are analysed. In the process, several forms of attractors and bifurcation patterns are seen. The stability zones are enumerated with the help of the bi-parametric Lyapunov plots or shrimp structures. Lastly, we have analysed the behaviour of two such coupled systems for the analysis of different modes of synchronization. The coupling is chosen in different ways. One is the direct one, the other through quorum sensing and lastly through delayed quorum sensing. It is observed that introduction of delay effects the time to achieve synchronization. In each case, the stability and other properties are analysed.

DOI:10.5506/APhysPolB.48.1529

1. Introduction

Chaotic behaviour of nonlinear systems has drawn wide attention over the last few decades. Examples of such systems are now found in the domain of physical sciences, chemical engineering, economics and many more [1–5]. An important class of problems occurs in the field of nonlinear optics which has become a subject of paramount importance due to its application in the communication technology. Optical parametric oscillators has also grabbed the attention due to its broadly tunable sources of highly coherent radiation. Subharmonic conversion inside a resonant cavity pumped by an external laser is called an optical parametric oscillator (OPO), when the subharmonic field has infinite intensity [6]. The elementary process which takes place in the OPO is the absorption of one photon of pump field at frequency 2ω and emission of two photons at frequencies ω_1 and ω_2 with energy conversion law $2\omega = \omega_1 + \omega_2$. When $\omega_1 = \omega_2$, the system is called degenerate optical parametric oscillator or DOPO. Different field polarization makes the two beams separable. DOPO finds its applications in various fields:

(1) As a model system for the generation of non-classical states of light [7, 8].

(2) It was demonstrated that light squeezing can occur between the two emitted beams [9, 10].

(3) It also acts as a simple model for a non-equilibrium phase transition [11].

In this context, researchers are studying pattern formation, spatial solitons, localized states in DOPO [12–15]. The existence of domain wall in such systems has been analysed and dissipative localized structures have been studied. In general, an optical parametric oscillator is obtained by filling an optical cavity with a nonlinear quadratic medium. They have variation both with respect to space and time. The pattern formation which occurs in hydrodynamics, chemistry, biology can be observed in these systems. It is interesting to note that such systems include both classical and quantum effects. The DOPO is actually effective as a laser wavelength doubler which is useful for pumping [16].

Another interesting aspect of these systems is that on the one hand, they support formation of soliton but in different parameter domain, they show instability and chaos. Important work has been done by Oppo *et al.* [12] and Stalinuas *et al.* [15] regarding their spatio-temporal behaviour. But if spatial variations are neglected, one still obtains important dynamical features. Here, in this communication, we have analysed the temporal evolution of such a degenerate optical parametric oscillator system and have visualized different routes to chaos and bifurcation. The stability zones are

analysed with the help of bi-parametric plots of the Lyapunov exponents. In the next stage, we have coupled two such systems for obtaining synchronization. Synchronization is another highly researched topic for the last few decades [17, 18]. Two types of synchronization exits in nonlinear dynamic systems — chaotic and nonchaotic. Communication through periodic synchronization and its security has been explored by various researchers [19–21]. Quasi-periodic synchronization of dynamical systems was studied by Ramaswamy [22]. To achieve synchronization, two types of couplings have been used — one through the direct process and the other through quorum sensing. In each case, the features of the coupled system are studied and condition for synchronization is established.

2. Basic dynamical behaviour of DOPO

Degenerate optical parametric oscillator is actually the temporal part of the laser equation describing the cavity dynamics occurring in nonlinear optics. Let A_1 and A_0 denote the complex amplitudes of subharmonic and fundamental mode of the field, and Δ_1 and Δ_0 denote the detuning parameters, γ is the reduced decay rate of the fundamental mode and E_{A} is the input field amplitude chosen as real and positive. Then the DOPO can be written as

$$\begin{aligned} \frac{\mathrm{d}A_1}{\mathrm{d}t} &= -(1+i\Delta_1)A_1 + A_1^* A_0\,, \\ \frac{\mathrm{d}A_0}{\mathrm{d}t} &= -(\gamma+i\Delta_0)A_0 + E_{\mathrm{A}} - A_1^2\,. \end{aligned} \tag{2.1}$$

If we set $A_1 = x + iy$ and $A_0 = u + iv$, then (2.1) reduces to

$$\begin{aligned} \frac{\mathrm{d}x}{\mathrm{d}t} &= -x + \Delta_1 y + xu + yv\,, \\ \frac{\mathrm{d}y}{\mathrm{d}t} &= -\Delta_1 x - y - yu + xv\,, \\ \frac{\mathrm{d}u}{\mathrm{d}t} &= -\gamma u + \Delta_0 v - x^2 + y^2 + E_{\mathrm{A}}\,, \\ \frac{\mathrm{d}v}{\mathrm{d}t} &= -\gamma v - \Delta_0 u - 2xy\,. \end{aligned} \tag{2.2}$$

Before proceeding to numerical analysis, the simple fixed point can be obtained as

$$x = y = 0\,; \qquad u = \frac{\gamma E_{\mathrm{A}}}{\Delta_0^2 + \gamma^2}\,; \qquad v = \frac{\Delta_0 E_{\mathrm{A}}}{\Delta_0^2 + \gamma^2}\,. \tag{2.3}$$

Another one is

$$v = 0\,, \qquad u^2 = \Delta_0^2 + 1\,, \tag{2.4}$$

$$2x^2 = (E_{\rm A} - \gamma u) \pm \sqrt{(E_{\rm A} - \gamma u)^2 + \Delta_0^2 u^2}\,, \tag{2.5}$$

$$-2y^2 = (E_{\rm A} - \gamma u) \mp \sqrt{(E_{\rm A} - \gamma u)^2 + \Delta_0^2 u^2}\,. \tag{2.6}$$

Similarly, one can have

$$u = 0\,, \qquad v^2 = \Delta_1^2 + 1 \tag{2.7}$$

with the corresponding complicated expression for x and y.

As far as stability is concerned, these analytic expressions do not convey much except for the first fixed point. The characteristic roots of the corresponding Jacobian are

$$\lambda = -\gamma \pm i\Delta_0\,, \tag{2.8}$$

$$\lambda + 1 = \pm\left(u^2 - v^2 + \Delta_1^2\right)^{1/2}\,, \tag{2.9}$$

where u, v are given in Eq. (2.3), which shows the existence of the Hopf bifurcation and stability depending on parameter values. Such a treatment is not feasible for the other set given in Eq. (2.6), so from here, we proceed numerically.

Numerical integration of the system with the Runge–Kutta algorithm leads to the form of the attractors as shown in figure 1 (a)–(d), where different two-dimensional projections are exhibited.

The phase-space structure depends crucially on the input field amplitude $E_{\rm A}$. For example, in figure 2 (a), we show a single period orbit for $E_{\rm A} = 5.4$, but for a slight change of value of $E_{\rm A} = 5.5$, we get the multiperiodic structure in figure 2 (b). But for $E_{\rm A} = 6.0$, we get back the full attractor as shown in figure 2 (c) which further enlarges in size when the value of $E_{\rm A} = 8.0$, as depicted in figure 2 (d). To analyse the stability, the bifurcation diagrams with respect to different parameters of the system and the corresponding Lyapunov exponents are also calculated. The bifurcation and the corresponding variation of the Lyapunov exponents with respect to parameter γ are shown in figures 3 (a) and (b), where all the exponents are negative. The situation changes when the varying parameter is chosen to be Δ_0. In this case, a small positive value is attained. The corresponding situations for variations with Δ_0 are given in figures 3 (c) and (d). Lastly, the most important parameter, $E_{\rm A}$, is taken into account and the bifurcation diagram, and the Lyapunov exponent variation with respect to $E_{\rm A}$ are depicted in figures 3 (e) and (f).

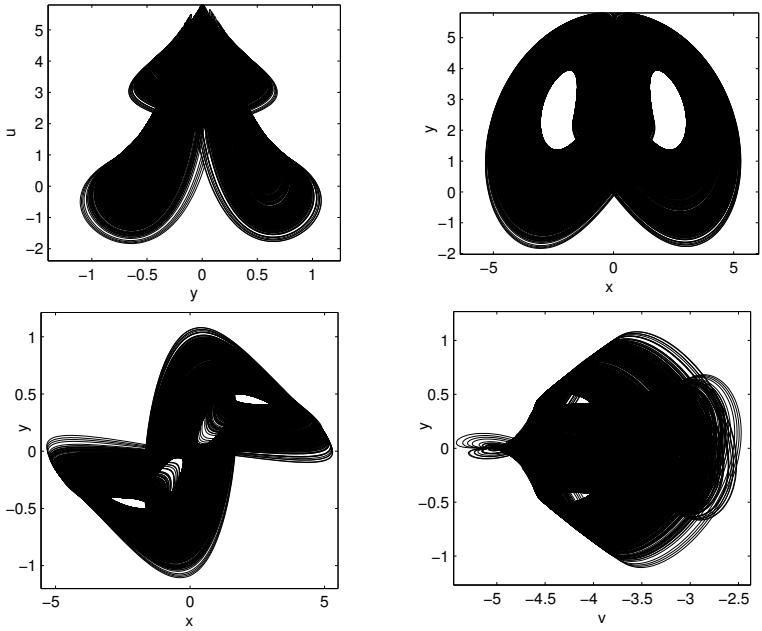

Fig. 1. Attractors arising from Eq. (2.2).

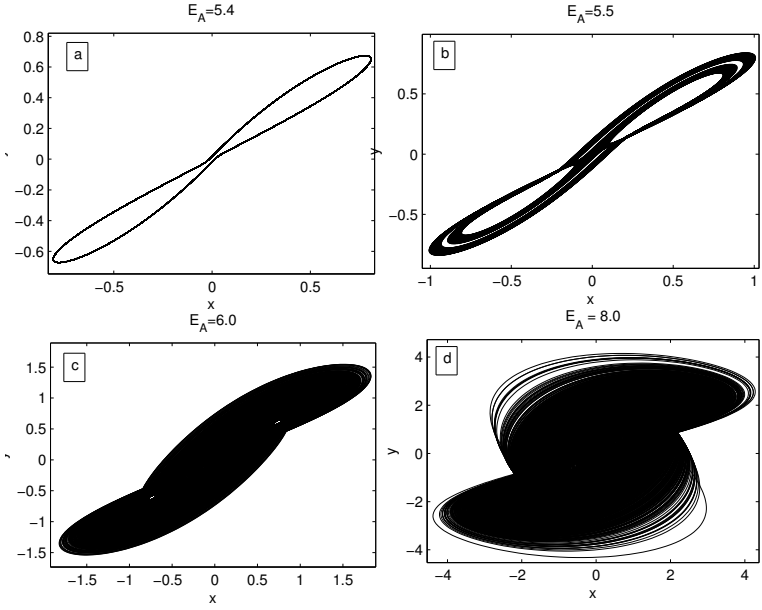

Fig. 2. Variation in the attractors with the change of E_{A}.

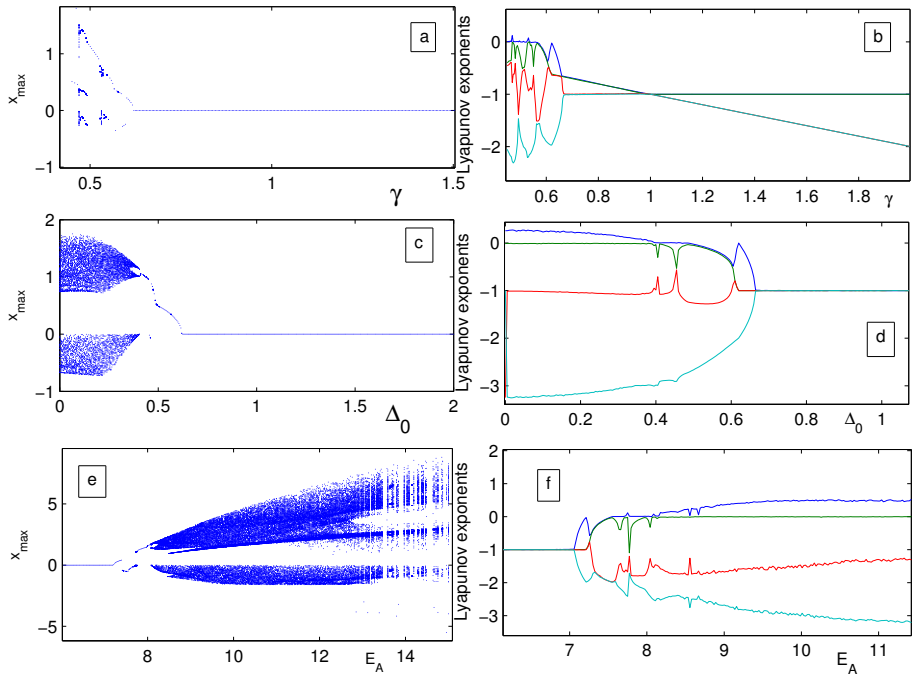

Fig. 3. Bifurcation diagrams and Lyapunov exponents w.r.t. different system parameters.

3. Stability properties

In the previous section, for DOPO system, we have encountered the existence of quite a few number of fixed points, both trivial and non-trivial. As the system depends on a large number of parameters, the eigenvalues corresponding to these fixed points can always change their character and hence the type of stability properties. Actually, the local stability can be ascertained by these eigenvalues but the stability as a whole can only be estimated through the computation of the Lyapunov exponents. In this section, we report on the computational results of the Lyapunov exponents for the original and various forms of the coupled type DOPO equations. The system stability may reveal different scenario depending on the choice of parameter values. The bifurcation structure indicates a change of qualitative behaviour when system parameters are varied. Recently, a new type of bifurcation structures are reported in many types of discrete and continuous nonlinear dynamical systems, when two or more control parameters are varied. The parameter-planes show iso-periodic stable structures which are referred to as shrimp-shaped domains (SSDs), with a variety of bifurcation cascades and organization rules. Many researchers have unveiled the detailed bifurcation

structures in the parameter-planes of different nonlinear systems [26–30]. The periodic islands in the chaotic domain in the bi-parametric plots are observed by considering the largest Lyapunov exponent. Such plots are first done for the single DOPO system and with various combinations of system parameters. In each case, an array of 500×500 points has been considered. The results are shown in figure 4 (a)–(f). In figure 4 (a), we have the parameter space of E_{A} *versus* γ. It shows chaotic islands mainly for higher values of E_{A}, although we can observe an island for low E_{A} and γ. The periodic region is restricted to lower values of E_{A} only. The plot of Δ_1 *versus* γ

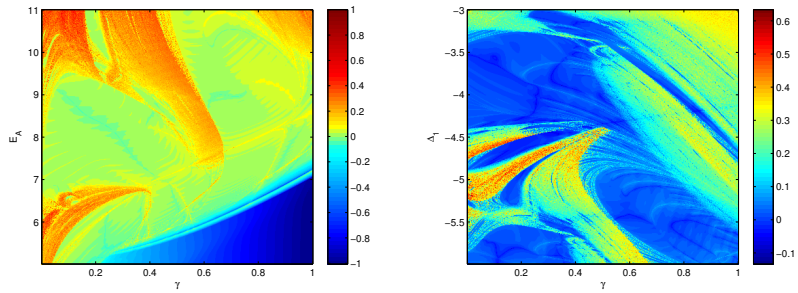

(a) Plot of E_{A} *versus* γ.

(b) Plot of Δ_1 *versus* γ.

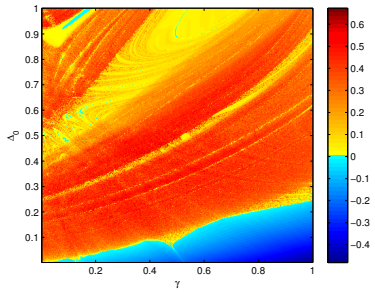

(c) Plot of Δ_0 *versus* γ.

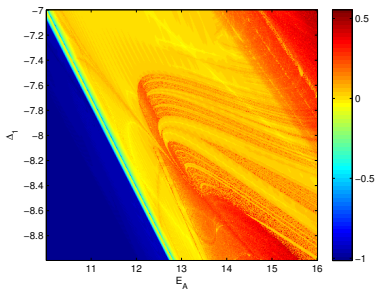

(d) Plot of Δ_1 *versus* E_{A}.

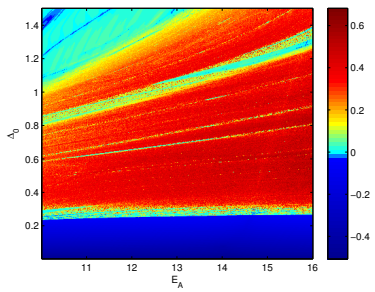

(e) Plot of Δ_0 *versus* E_{A}.

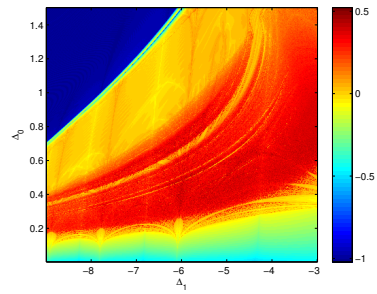

(f) Plot of Δ_0 *versus* Δ_1.

Fig. 4. Bi-parametric plots of different combination of parameters of the system given by Eq. (2.2).

(figure 4 (b)) shows mainly periodic regimes, while Δ_0 *versus* γ (figure 4 (c)) shows the dominance of chaotic regions. Δ_1 *versus* E_A (figure 4 (d)) shows chaotic dynamics after $E_A = 12.6$, while in Δ_0 *versus* E_A (figure 4 (e)) chaotic islands appear after $\Delta_0 = 0.3$ for any value of E_A. Δ_1 *versus* Δ_0 (figure 4 (f)) shows that for lower values of Δ_0, periodicity occurs thereafter giving rise to chaoticity which gradually decreases for higher values of Δ_0.

Next, the case of coupled systems (the details of which is discussed in Section 4) is considered. Firstly, two DOPO systems are directly coupled to one another through a coupling constant of certain strength. The system variables are directly involved in the process and the dynamics of the second system becomes dependent on the first. Next, quorum sensing (QS) is inspected which is a sort of indirect coupling because interaction takes place through another dynamical environment. To critically understand the onset of periodic and chaotic motions in this coupled system, one needs to analyse at least the first four Lyapunov exponents in detail for different parameter variations. This is best described by bi-parametric plots as they indicate the parameter regions where synchronization occurs by taking into account the transverse Lyapunov exponent. These are given in figure 5 (a)–(d) where the synchronization takes place due to direct coupling. The governing system

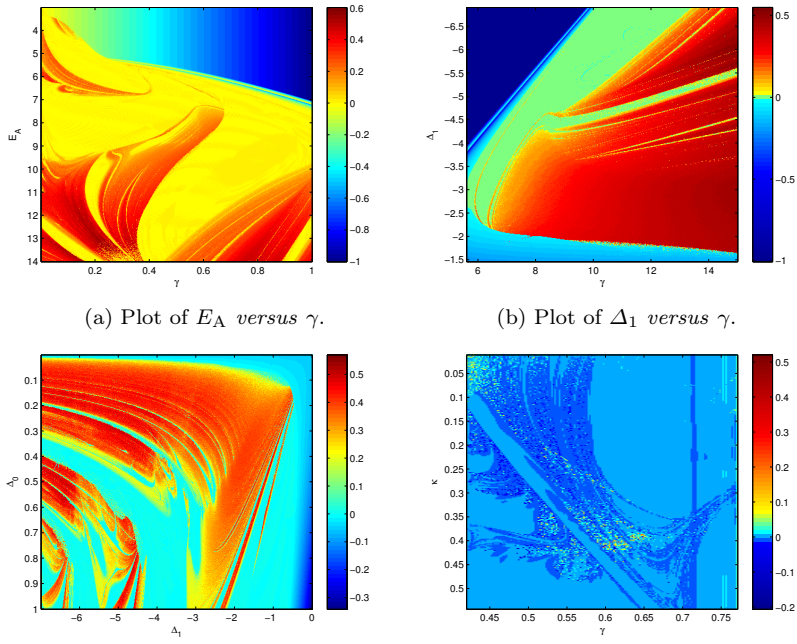

(a) Plot of E_A *versus* γ.

(b) Plot of Δ_1 *versus* γ.

(c) Plot of Δ_0 *versus* Δ_1.

(d) Plot of κ *versus* γ.

Fig. 5. Bi-parametric plots of different combination of parameters of directly coupled DOPO system given by Eq. (4.1).

of equations in this case is given by Eq. (4.1). In this case of coupling, we have chosen four pairs of parameters. In figure 5 (a), for E_A *versus* γ, we observe that the transverse Lyapunov exponent becomes negative *i.e.*, synchronization sets in completely for $E_A = 8.0$. For Δ_1 *versus* γ (figure 5 (b)), synchronization occurs mainly for lower values of Δ_1 and γ. Plot of Δ_1 *versus* Δ_0 (figure 5 (c)) shows scattered islands of unsynchronized state in the synchronized basin. Lastly, in κ *versus* γ (figure 5 (d)), we see that in the region $0.04 < \kappa < 0.6$, we have the synchronized regime.

In the second case, the governing equations indicating quorum sensing synchronization are described by Eq. (4.2). The plots for quorum sensing coupling are shown in figure 6 (a)–(d). In this case, we have also chosen four pairs of parameters to depict the stability of synchronization and observed that all of them indicate a rich form of dynamics. In the first case of E_A and γ (figure 6 (a)), we can see mostly synchronized regions. The same is for the case of Δ_1 *versus* γ (figure 6 (b)) where we see few islands of unsynchronized state. The effect of κ is depicted in figures 6 (c) and (d). The black/blue regions indicate the totally synchronized state of the two systems.

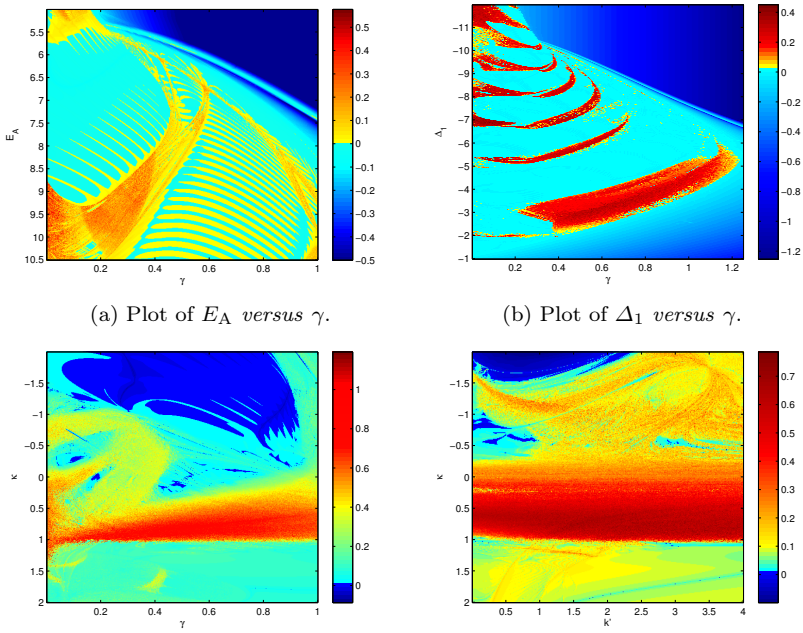

(a) Plot of E_A *versus* γ.

(b) Plot of Δ_1 *versus* γ.

(c) Plot of κ *versus* γ.

(d) Plot of κ *versus* k'.

Fig. 6. (Color online) Bi-parametric plots of different combination of parameters of coupled DOPO system through quorum sensing given by Eq. (4.2).

4. Synchronization of DOPO systems

In this section, behaviour of two coupled DOPO systems is studied to observe the phenomenon of synchronization. Synchronization of chaotic systems is very intriguing and displays interesting results when nonlinear optical systems are involved. Here, one of the DOPO systems is considered to be the drive and a similar one as the response system. We know that two systems can be coupled in various ways. Firstly, we consider the case when the two systems are directly coupled to one another through a coupling constant of a certain strength. The system variables gets directly involved and one system governs the dynamics of the other. The governing equations can be written as following when two variables have been engaged in coupling process:

$$\begin{aligned}
\frac{\mathrm{d}x}{\mathrm{d}t} &= -x + \Delta_1 y + xu + yv\,,\\
\frac{\mathrm{d}y}{\mathrm{d}t} &= -\Delta_1 x - y - yu + xv\,,\\
\frac{\mathrm{d}u}{\mathrm{d}t} &= -\gamma u + \Delta_0 v - x^2 + y^2 + E_{\mathrm{A}}\,,\\
\frac{\mathrm{d}v}{\mathrm{d}t} &= -\gamma v - \Delta_0 u - 2xy\,,\\
\frac{\mathrm{d}p}{\mathrm{d}t} &= -p + \Delta_1 q + pr + qs - \kappa(p - x)\,,\\
\frac{\mathrm{d}q}{\mathrm{d}t} &= -\Delta_1 p - q - qr + ps - \kappa(q - y)\,,\\
\frac{\mathrm{d}r}{\mathrm{d}t} &= -\gamma r + \Delta_0 s - p^2 + q^2 + E_{\mathrm{A}}\,,\\
\frac{\mathrm{d}s}{\mathrm{d}t} &= -\gamma s - \Delta_0 r - 2pq\,,
\end{aligned} \tag{4.1}$$

where κ is the coupling constant. One achieves a synchronized state when two systems are coupled in this form and the results of error plot of $[x(t) - p(t)]$ are illustrated in figure (7). After synchronization as both the systems are behaving in the similar way, when we plot the phase space with variables as q *versus* x, an attractor given in figure (8) shows up.

Next, we have considered the coupling in a different way — namely quorum sensing (QS). In nature, it is seen that communication through synchronization between individual elements does not occur directly, but rather through a dynamical environment [23]. The QS is quite common in oscillator systems with homogeneous environment and may be observed in heterogeneous environment too. Bacteria, for instance, produce, release and sense signalling molecules which can diffuse in the environment and are used for the population coordination. This quorum sensing mechanism [24]

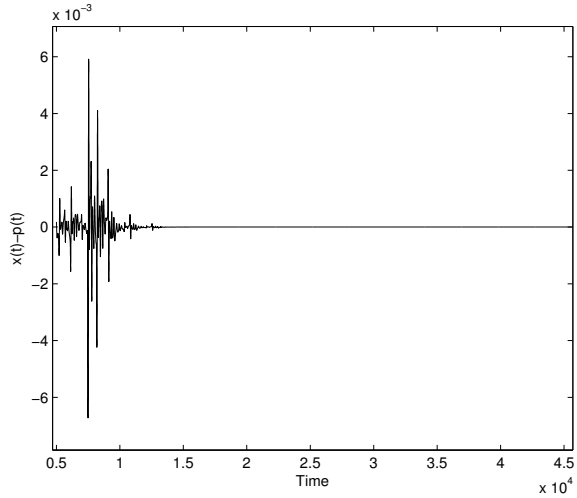

Fig. 7. Error dynamics of coupled DOPO system through direct coupling.

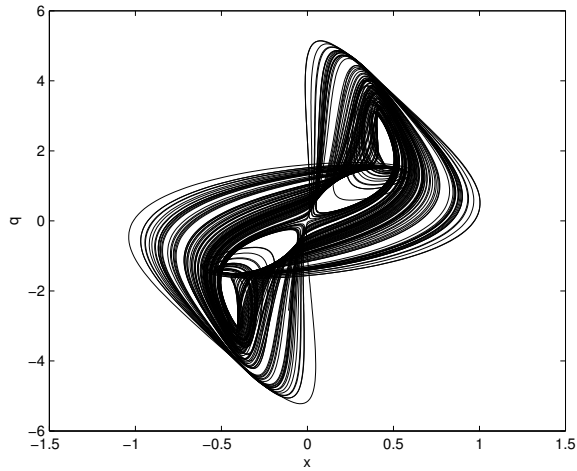

Fig. 8. Phase space plotted with cross variables from two systems.

is believed to play a key role in bacterial infection, bioluminescence and biofilm formation [25]. The coupling of DOPO systems via quorum sensing gives the following set of equations:

$$\begin{aligned} \frac{\mathrm{d}x}{\mathrm{d}t} &= -x + \Delta_1 y + xu + yv - \kappa(z - x)\,, \\ \frac{\mathrm{d}y}{\mathrm{d}t} &= -\Delta_1 x - y - yu + xv - \kappa(w - y)\,, \end{aligned}$$

$$\begin{aligned}
\frac{\mathrm{d}u}{\mathrm{d}t} &= -\gamma u + \Delta_0 v - x^2 + y^2 + E_\mathrm{A}\,,\\
\frac{\mathrm{d}v}{\mathrm{d}t} &= -\gamma v - \Delta_0 u - 2xy\,,\\
\frac{\mathrm{d}p}{\mathrm{d}t} &= -p + \Delta_1 q + pr + qs - \kappa(z-p)\,,\\
\frac{\mathrm{d}q}{\mathrm{d}t} &= -\Delta_1 p - q - qr + ps - \kappa(w-q)\,,\\
\frac{\mathrm{d}r}{\mathrm{d}t} &= -\gamma r + \Delta_0 s - p^2 + q^2 + E_\mathrm{A}\,,\\
\frac{\mathrm{d}s}{\mathrm{d}t} &= -\gamma s - \Delta_0 r - 2pq\,,\\
\frac{\mathrm{d}z}{\mathrm{d}t} &= k'(x - 2z + p)/2 - gz\,,\\
\frac{\mathrm{d}w}{\mathrm{d}t} &= k'(y - 2w + q)/2 - gw\,. \qquad (4.2)
\end{aligned}$$

Two systems get coupled via (z, w) which refer to the indirect coupling. Integrating again numerically, synchronization between the two systems coupled through quorum sensing, is achieved. The error plot is shown in figure 9 and the projection of the attractor obtained by plotting q *versus* x is shown in figure 10. One may note that, in this case, the synchronization takes a longer time to set in.

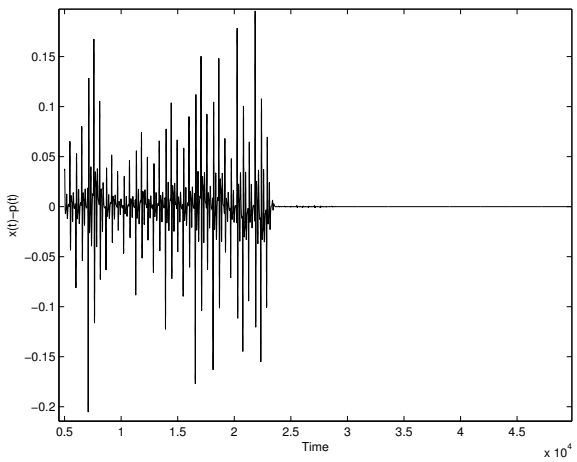

Fig. 9. Error dynamics of coupled DOPO system through quorum sensing.

Exploring further with quorum sensing synchronization, the effect of delay in the coupling is considered. This can point to the condition, where the effect of coupling, which is indirect, is occurring after a certain time

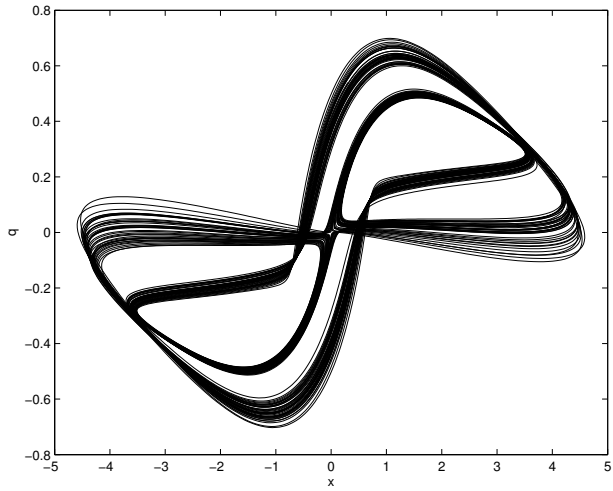

Fig. 10. Phase space plotted with cross variables from two systems.

span. The equations in this case can be written as:

$$\begin{aligned}
\frac{\mathrm{d}x}{\mathrm{d}t} &= -x + \Delta_1 y + xu + yv - \kappa(z(t-\tau) - x)\,, \\
\frac{\mathrm{d}y}{\mathrm{d}t} &= -\Delta_1 x - y - yu + xv - \kappa(w(t-\tau) - y)\,, \\
\frac{\mathrm{d}u}{\mathrm{d}t} &= -\gamma u + \Delta_0 v - x^2 + y^2 + E_\mathrm{A}\,, \\
\frac{\mathrm{d}v}{\mathrm{d}t} &= -\gamma v - \Delta_0 u - 2xy\,, \\
\frac{\mathrm{d}p}{\mathrm{d}t} &= -p + \Delta_1 q + pr + qs - \kappa(z(t-\tau) - p)\,, \\
\frac{\mathrm{d}q}{\mathrm{d}t} &= -\Delta_1 p - q - qr + ps - \kappa(w(t-\tau) - q)\,, \\
\frac{\mathrm{d}r}{\mathrm{d}t} &= -\gamma r + \Delta_0 s - p^2 + q^2 + E_\mathrm{A}\,, \\
\frac{\mathrm{d}s}{\mathrm{d}t} &= -\gamma s - \Delta_0 r - 2pq\,, \\
\frac{\mathrm{d}z}{\mathrm{d}t} &= k'(x - 2z + p)/2 - gz\,, \\
\frac{\mathrm{d}w}{\mathrm{d}t} &= k'(y - 2w + q)/2 - gw\,. \qquad (4.3)
\end{aligned}$$

The delay is associated with the variables which contribute to the indirect coupling, namely, z and w. The system is first run with $\tau = 0.0$ and then

with $\tau = 0.5$. The observations are shown in figure 11. It is interesting to note that synchronization is achieved in both cases, but with $\tau = 0.5$ the synchronization sets in much earlier in comparison to $\tau = 0.0$. This may be due to the fact that delay acts like a feedback in optical systems which induces a control-like effect in the process.

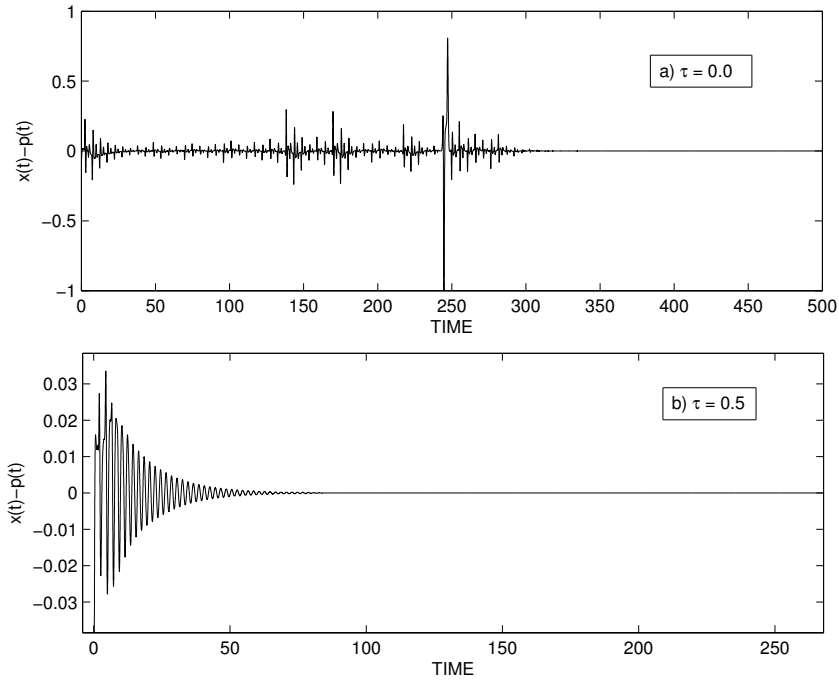

Fig. 11. Synchronization with delayed quorum sensing of two DOPO systems.

5. Conclusion

In the present communication, the complex dynamics underlying a degenerate optical parametric oscillator system is analysed by considering only the temporal behaviour of the original partial differential equations. The domain of the equation, nonlinear optics, though is a highly researched field yet very few work can be found dealing with their stability and synchronization. Our analysis reveals the inner hidden properties of such systems and can be of use for actual practical purposes. Rich chaotic dynamics is exhibited in such systems and these properties get unfolded through phase space diagrams, bifurcations and the Lyapunov exponents. The entire parameter region is explored for the stability analysis through the help of bi-parametric plots indicating the actual regions for the possibility of syn-

chronization. Since nonlinear optics is related to communication process, such analysis can turn useful for actual data transmission and signal processing. The various modes of coupling hold relevance in various biological processes. One such mode is the synchronization through quorum sensing which indicates interaction via dynamical environment.

REFERENCES

[1] S.H. Strogatz, *Nonlinear Dynamics and Chaos: with Applications to Physics, Biology, Chemistry, and Engineering*, Westview Press, 2014.

[2] J. Guckenheimer, P. Holmes, *Nonlinear Oscillations, Dynamical Systems and Bifurcations of Vector Fields*, Springer, New York 1983.

[3] S. Boccaletti *et al.*, *Phys. Rep.* **424**, 175 (2006).

[4] N.V. Kuznetsov, *Lect. Notes Electr. Eng.* **371**, 13 (2016).

[5] G.A. Leonov, N.V. Kuznetsov, T.N. Mokaev, *Eur. Phys. J. Spec. Top.* **224**, 1421 (2015).

[6] N.P. Pettiaux, R.-D. Li, P. Mandel, *Opt. Commun.* **72**, 256 (1989).

[7] B.R. Mollow, *Phys. Rev. A* **8**, 2684 (1973).

[8] D. Stoler, *Phys. Rev. Lett.* **33**, 1397 (1974).

[9] L.I. Plimak, D.F. Walls, *Phys. Rev. A* **50**, 2627 (1994).

[10] S. Chaturvedi, K. Dechoum, P.D. Drummond, *Phys. Rev. A* **65**, 033805 (2002).

[11] T. Leleu, Y. Yamamoto, S. Utsunomiya, K. Aihara, *Phys. Rev. E* **95**, 022118 (2017).

[12] G.L. Oppo, M. Brambilla, L.A. Lugiato, *Phys. Rev. A* **49**, 2028 (1994).

[13] V.B. Taranenko, K. Staliunas, C.O. Weiss, *Phys. Rev. Lett.* **81**, 2236 (1998).

[14] S. Trillo, M. Haelterman, A. Sheppard, *Opt. Lett.* **22**, 970 (1997).

[15] K. Staliunas, V.J. Sanchez-Morcillo, *Phys. Rev. A* **57**, 1454 (1998).

[16] K. Hayasaka, Y. Zhang, K. Kasai, *Opt. Lett.* **29**, 1665 (2004).

[17] L.M. Pecora, T.L. Carroll, *Chaos* **25**, 097611 (2015).

[18] A. Pikovsky, M. Rosenblum, J. Kurths, *Synchronization: A Universal Concept in Nonlinear Sciences*, Vol. 12. Cambridge University Press, 2003.

[19] K. Murali, M. Lakshmanan, *Phys. Lett. A* **241**, 303 (1998).

[20] L. Kocarev, U. Parlitz, *Phys. Rev. Lett.* **74**, 5028 (1995).

[21] K.M. Cuomo, A.V. Oppenheim, S.H. Strogatz, *IEEE Trans. Circuits Syst. II Analog Digit. Signal Process.* **40**, 626 (1993).

[22] R. Ramaswamy, *Phys. Rev. E* **56**, 7294 (1997).

[23] G. Russo, J.J.E. Slotine, *Phys. Rev. E* **82**, 041919 (2010).

[24] M. Miller, B. Bassler, *Annu. Rev. Microbiol.* **55**, 165 (2001).

[25] C. Anetzberger, T. Pirch, K. Jung, *Mol. Microbiol.* **73**, 267 (2009).

[26] A. Hoff, Denilson T. da Silva, C. Manchein, H.A. Albuquerque, *Phys. Lett. A* **378**, 171 (2014).

[27] D.F.M. Oliveira, E, D. Leonel, *Physica A* **392**, 1762 (2013).

[28] C. Stegemann, H.A. Albuquerque, R.M. Rubinger, P.C. Rech, *Chaos* **21**, 033105 (2011).

[29] W. Facanha, B. Oldeman, L. Glass, *Phys. Lett. A* **377**, 1264 (2013).

[30] R.E. Francke, T. Pöschel, J.A.C. Gallas, *Phys. Rev. E* **87**, 042907 (2013).